Electronic Supplementary Material (ESI) for Physical Chemistry Chemical Physics.


# Electronic Supplementary Information

## A Fullerene-Carbene Adduct as a Crystalline Molecular Rotor: Remarkable Behavior of a Spherically-Shaped Rotator

Andreas Lorbach*, Emily Maverick, Abel Carreras, Pere Alemany, Guang Wu, Miguel A. Garcia-Garibay*, Guillermo C. Bazan*

**Procedure for the crystallization of 1**

The synthesis and crystallization of **1** were carried out under an $N_2$ atmosphere using glove box techniques. Chloronaphthalene (isomer mixture of 90% 1-chloronaphthalene and 10% 2-chloronaphthalene) and toluene were freshly distilled from $CaH_2$ and Na/benzophenone, respectively.

A solution of fullerene $C_{60}$ (100.0 mg, 0.1388 mmol) in chloronaphthalene (13.0 g) was treated with 1,3-bis(diisopropylphenyl)imidazol-2-ylidene (54.5 mg, 0.140 mmol) and stirred at room temperature for 10 min. The mixture was then filtered (cellulose acetate syringe filter, pore size: 0.2 µm) and the filtrate was collected. Crystals of **1**, suitable for X-ray crystallography, were obtained within 7 d at room temperature by (i) adding toluene (15 g) to an aliquot of the filtrate (3 g) or (ii) vapor diffusion of toluene into the filtrate.

**Table S1**. Selected crystallographic data for **1**.

| compound | {**1**} (VT experiment) | | | | | | | | | {**1**} | {**1**(tol)$_2$} | {**1**(CNPT)$_2$} |
|---|---|---|---|---|---|---|---|---|---|---|---|---|
| formula | $C_{87}H_{36}N_2$ | | | | | | | | | $C_{87}H_{36}N_2$ | $C_{87}H_{36}N_2 \cdot 2\,C_7H_8$ | $C_{87}H_{36}N_2 \cdot 2\,C_{10}H_7Cl$ |
| fw | 1109.18 | | | | | | | | | 1109.18 | 1293.45 | 1434.39 |
| radiation, $\lambda$ [Å] | Mo$K_\alpha$, 0.71073 | | | | | | | | | Mo$K_\alpha$, 0.71073 | Mo$K_\alpha$, 0.71073 | Mo$K_\alpha$, 0.71073 |
| crystal system | orthorhombic | | | | | | | | | ortho-rhombic | monoclinic | triclinic |
| space group | *Pnma* | | | | | | | | | *Pnma* | $P2_1/c$ | $P$-1 |
| $T$ [K] | 80(2) | 130(2) | 180(2) | 230(2) | 280(2) | 330(2) | 380(2) | 430(2) | 480(2) | 100(2) | 100(2) | 130(2) |
| $a$ [Å] | 18.4633(8) | 18.4939(8) | 18.5461(8) | 18.5990(7) | 18.6446(7) | 18.7040(15) | 18.7596(17) | 18.810(2) | 18.833(4) | 18.4290(8) | 14.5190(8) | 12.6739(15) |
| $b$ [Å] | 18.1906(6) | 18.2041(6) | 18.2325(6) | 18.2650(6) | 18.2957(6) | 18.3030(12) | 18.3558(13) | 18.4239(18) | 18.483(4) | 18.1729(13) | 19.3733(11) | 14.0712(16) |
| $c$ [Å] | 15.0501(7) | 15.0446(7) | 15.0393(7) | 15.0367(7) | 15.0193(7) | 14.9839(13) | 14.9944(15) | 15.008(2) | 14.978(4) | 15.0366(8) | 22.0000(13) | 19.438(2) |
| $\alpha$ [°] | 90 | | | | | | | | | 90 | 90 | 102.258(3) |
| $\beta$ [°] | 90 | | | | | | | | | 90 | 93.8870(10) | 97.661(3) |
| $\gamma$ [°] | 90 | | | | | | | | | 90 | 90 | 104.351(3) |
| $V$ [Å$^3$] | 5054.7(4) | 5065.0(4) | 5085.4(4) | 5108.1(3) | 5123.3(3) | 5129.6(7) | 5163.3(8) | 5201.1(11) | 5214(2) | 5035.9(5) | 6173.9(6) | 3217.9(6) |
| $Z$ | 4 | | | | | | | | | 4 | 4 | 2 |
| $D_{calcd}$ [g cm$^{-3}$] | 1.458 | 1.455 | 1.449 | 1.442 | 1.438 | 1.436 | 1.427 | 1.417 | 1.413 | 1.463 | 1.392 | 1.480 |
| $F$(000) | 2288 | | | | | | | | | 2288 | 2688 | 1480 |
| crystal size [mm] | $0.3 \times 0.2 \times 0.1$ | | | | | | | | | $0.3 \times 0.3 \times 0.2$ | $0.4 \times 0.3 \times 0.2$ | $0.3 \times 0.3 \times 0.2$ |
| $\Theta$ range [°] | 1.75-28.27 | 1.74-28.26 | 1.74-28.23 | 1.74-28.22 | 1.74-28.27 | 1.74-28.26 | 1.74-28.33 | 1.74-28.30 | 1.74-28.43 | 1.75-26.38 | 1.40-30.64 | 1.09-28.57 |
| no. of rflns collected | 17583 | 17627 | 17632 | 17736 | 17849 | 17911 | 18139 | 18233 | 18323 | 41891 | 54477 | 25665 |
| no. of independent rflns ($R_{int}$) | 6269 (0.0282) | 6283 (0.0286) | 6285 (0.0310) | 6309 (0.0352) | 6357 (0.0384) | 6352 (0.0383) | 6419 (0.0418) | 6449 (0.0488) | 6503 (0.0700) | 5300 (0.0449) | 19020 (0.0292) | 15331 (0.0340) |
| data / restraints / parameters | 6269 / 0 / 413 | 6283 / 0 / 413 | 6285 / 0 / 413 | 6309 / 0 / 413 | 6357 / 0 / 413 | 6352 / 0 / 413 | 6419 / 0 / 413 | 6449 / 0 / 413 | 6503 / 0 / 413 | 5300 / 0 / 413 | 19020 / 0 / 981 | 15331 / 0 / 906 |
| GOF on $F^2$ | 1.031 | 1.012 | 1.016 | 1.002 | 1.046 | 1.030 | 1.047 | 1.018 | 0.986 | 1.052 | 1.026 | 1.061 |
| $R1$, $wR2$ ($I > 2\sigma(I)$) | 0.0439, 0.1057 | 0.0432, 0.1015 | 0.0424, 0.0980 | 0.0424, 0.0934 | 0.0489, 0.1179 | 0.0639, 0.1745 | 0.0796, 0.2336 | 0.0831, 0.2351 | 0.0807, 0.2499 | 0.0409, 0.0942 | 0.0519, 0.1291 | 0.1063, 0.2870 |
| $R1$, $wR2$ (all data) | 0.0617, 0.1169 | 0.0644, 0.1141 | 0.0670, 0.1117 | 0.0767, 0.1105 | 0.0914, 0.1397 | 0.1128, 0.2097 | 0.1487, 0.2915 | 0.1760, 0.3047 | 0.2133, 0.3476 | 0.0571, 0.1006 | 0.0752, 0.1437 | 0.1540, 0.3338 |
| largest diff. peak and hole [e Å$^{-3}$] | 0.372, −0.246 | 0.289, −0.225 | 0.223, −0.228 | 0.200, −0.212 | 0.318, −0.169 | 0.598, −0.224 | 0.724, −0.268 | 0.498, −0.273 | 0.266, −0.219 | 0.219, −0.210 | 0.677, −0.314 | 1.075, −0.920 |

**Table S2**. Distances between antipodal carbon atoms within the $C_{60}$ sphere of {**1**} (*T* = 100 K).

| **Atom1** | **Atom2** | **Distance [Å]** |
|---|---|---|
| C16 | C46 | 7.178(3) |
| C17 | C29 | 7.069(2) |
| C18 | C30 | 7.110(2) |
| C19 | C43 | 7.054(2) |
| C20 | C42 | 7.119(2) |
| C21 | C41 | 7.050(2) |
| C22 | C39 | 7.076(2) |
| C23 | C38 | 7.075(2) |
| C24 | C44 | 7.063(2) |
| C25 | C40 | 7.084(2) |
| C26 | C36 | 7.081(2) |
| C27 | C37 | 7.092(2) |
| C28 | C35 | 7.080(2) |
| C31 | C34 | 7.065(2) |
| C32 | C33 | 7.055(2) |
| **Average:** | | **7.08(3)** |
| **C15** | **C45** | **7.426(3)** |
| **Difference:** | | **0.35** |

$$I(A_n,T) = \frac{U_{eq}(A_n,T)}{U_{eq}(A_n,T\text{-}50\ \text{K})} \cdot n \cdot \left( \sum_n \frac{U_{eq}(A_n,T)}{U_{eq}(A_n,T\text{-}50\ \text{K})} \right)^{-1}$$

**Formula S1**. Definition of the relative increase $I(A_n,T)$ of $U_{eq}$ for the *n* non-hydrogen atoms $A_n$ of {**1**}. The parameters $I(A_n,T)$ at the different temperatures 130 K ≤ *T* ≤ 430 K were finally averaged for each atom $A_n$ to obtain the temperature-independent relative increase $I(A_n)$.

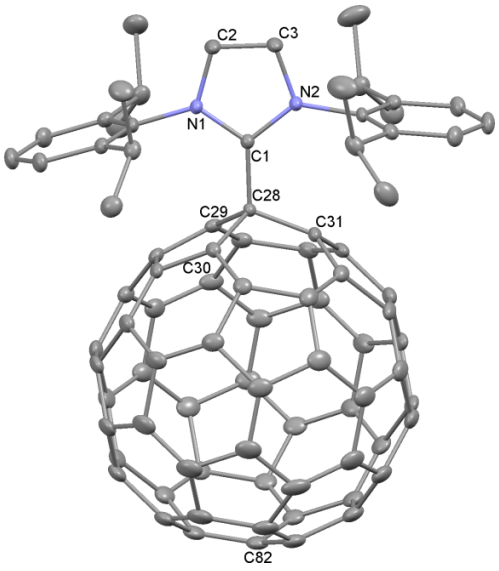


**Figure S1**. Molecular structure and numbering scheme in {**1**$(tol)_2$}; displacement ellipsoids are drawn at the 50% probability level; hydrogen atoms and toluene molecules are omitted for clarity; *T* = 100 K. The structure indicates disorder which was modeled as a rigid-body $C_{60}$ rotator constructed from the major conformer shown here (91.4% occupancy). Selected bond lengths [Å], atom···atom distance [Å], and (average) bond angles [°]: C1–C28 = 1.523(2), C1–N1 = 1.353(2), C1–N2 = 1.352(2), C2–N1 = 1.384(2), C3–N2 = 1.389(2), C2–C3 = 1.349(2), C28–C29 = 1.560(2), C28–C30 = 1.561(2), C28–C31 = 1.520(2); C28···C82 = 7.416(2); N1–C1–N2 = 106.3(1), C1–N1–C2 = 110.0(1), N1–C2–C3 = 106.9(1), C2–C3–N2 = 107.3(1), C1–N2–C3 = 109.5(1), C–C28–C = 109(5).

## THERMAL MOTION ANALYSIS OF SOLVENT-FREE {1}

### Overview

The crystal structure of {**1**} was determined at nine temperatures: 80, 130, 180, 230, 280, 330, 380, 430, and 480 K. At lower temperatures (80-230 or 280 K) the molecule could be treated as a rigid body for thermal motion analysis. The $C_{60}$ portion plus C1 in the imidazolium fragment was also studied as an independent molecule. At temperatures up to about 280 K, thermal motion analysis supports motion of the fullerene moiety relative to the imidazolium fragment with very good agreement factors. The greatest amplitude of libration of the fullerene corresponds to rotation about the axis C1-C15···C46, and these atoms are on the mirror plane in the space group *Pnma.*

As temperature increases above 300 K, Hirshfeld[i] tests indicate that the fullerene can no longer be considered a rigid body. The checkCIF/PLATON reports, commenting on the cifs we have prepared for deposit, raise several questions. A major complaint is the increasing number of Hirshfeld[i] test violations. There are two types of checks for these violations. The first type appears at 280 K: checkCIF notes violations if the ΔMSDA (calculated from the ADPs) in the bonded direction, between bonded atoms, exceeds 5 su (5 mesd(U)). There are five violations at 280 K involving the nine atoms in gray in Figure S2. The second type first appears at 380 K: in this test the Hirshfeld difference between bonded atoms is measured in Å, rather than by comparison with su values. Figure S2 shows the increase in all violations as the temperature increases. The su values themselves also increase dramatically with temperatures above 300 K (Figure S8, green curve), signifying errors in the determination of the ADPs.

If the assembly of atoms were librating as a rigid body, the Hirshfeld differences would be small, no greater than 2-3 su. If the test fails, the atomic positions do not represent the true locations of the atoms, nor can these positions be corrected by thermal motion analysis.

The ellipsoids cannot reliably be modeled as rigid-body motion (purely thermal disorder) at higher temperatures: they are probably evidence of positional disorder as well. CheckCIF notes unusual distances and angles. Bond lengths are "precise" to 0.01-0.02 Å at 430 K, whereas the precision in the fullerene is 0.002 Å at 80 K and 0.002-0.003 Å at 280 K.

At 480 K the structure can be solved in *Pnma* and in $Pna2_1$. In both space groups refinement results in indications of disorder, not only in the fullerene but also in the carbene moiety. We have tried some refinement with a disorder model, with little success so far.

CheckCIF also notes the presence of "solvent-accessible voids". The voids make the motion of the fullerene moiety possible, but as they increase in size with increasing temperature the contacts between molecules become longer and less restrictive. The calculated potential energies and the increasing disorder at higher temperatures indicate that additional energy minima are occupied. In the case of **1**, there is evidence from two other crystal structures that solvent molecules change the minimum-energy rotational positions for the $C_{60}$ moiety (Figure S3).

Thermal motion analysis shows that the fullerene is moving with respect to the imidazolium fragment, about the lengthened axis. The calculated libration amplitude of the fullerene about this axis is approximately proportional to temperatures from 80 to about 300 K. The libration amplitude (about $30(^\circ)^2$ at 300 K), and the rotational symmetry of close contacts (Figure S4), are combined to suggest approximate rotation barriers.

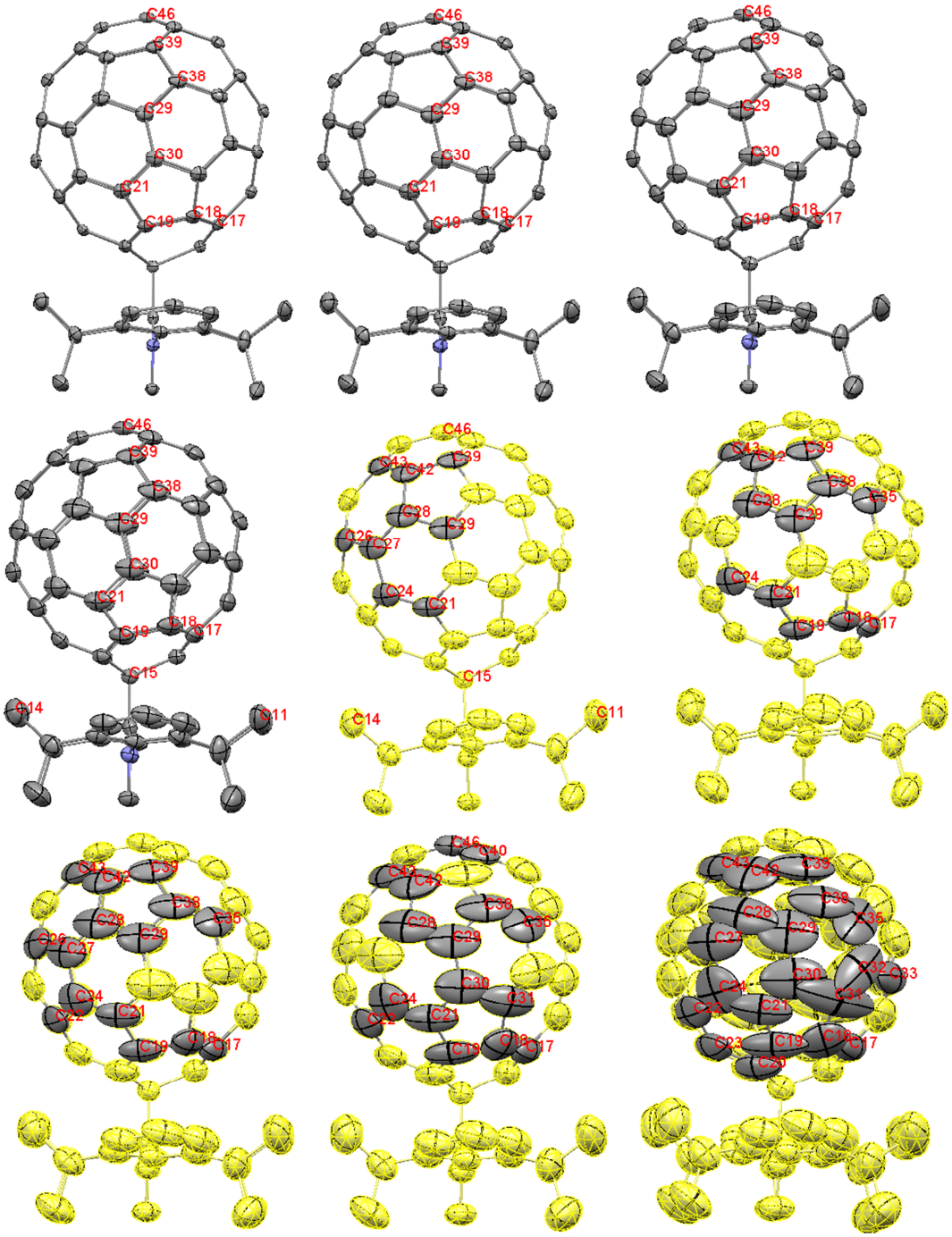

**Figure S2.** ADP ellipsoids (50% probability) for {**1**} at 80, 130, 180, 230, 280, 330, 380, 430, and 480 K (in order from top, left to right in each row). From 280 to 480 K, gray ellipsoids indicate atoms cited by checkCIF for Hirshfeld violations.[i] (Note: the numbering scheme is different for the variable-temperature structures; for the 100 K structure illustrated in Figure 1 (main text), the axial C atom is labeled C45.)

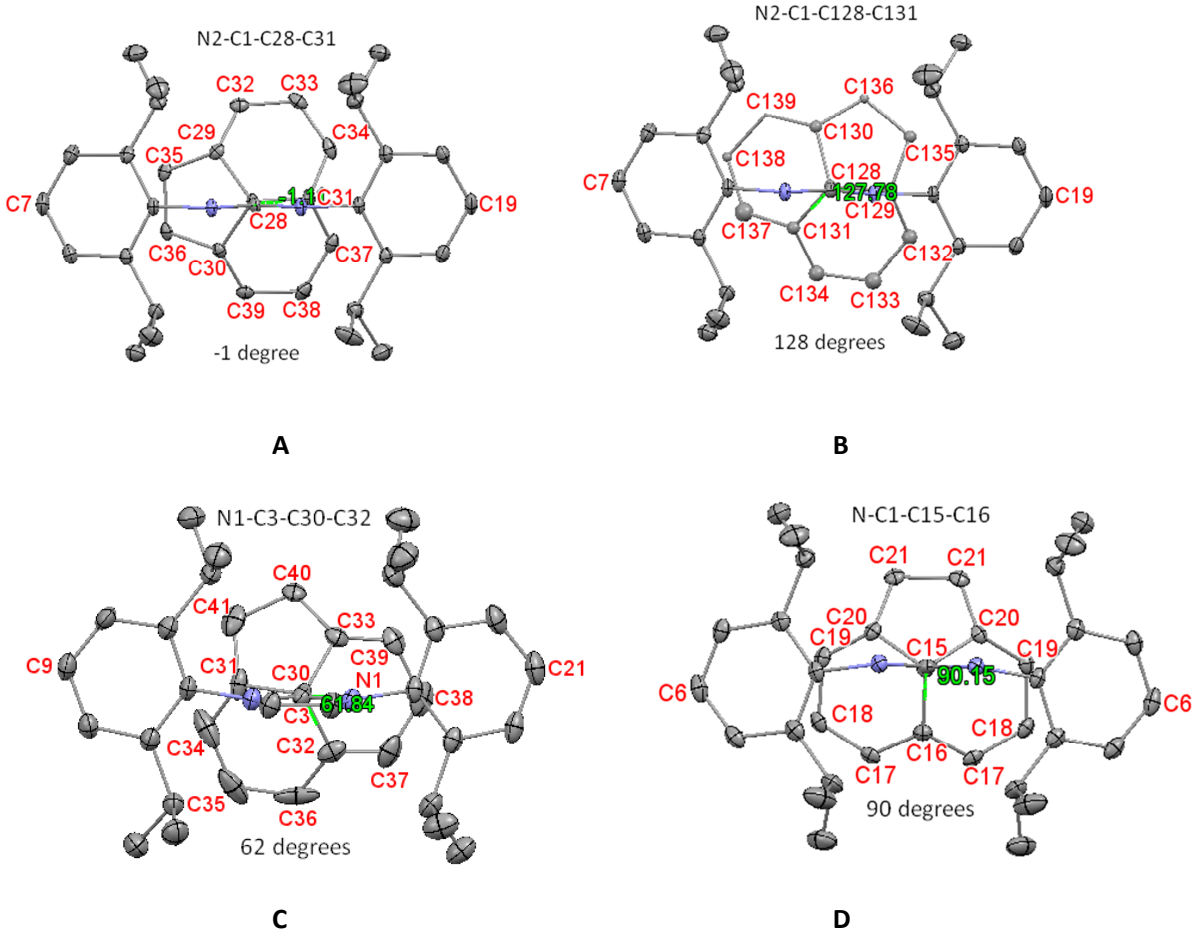


**Figure S3.** Rotator positions with respect to the stator for three pseudopolymorphs of **1**. **A**: {**1**(tol)$_2$}, major conformer (91.4%). Rotation position: –1°. **B**: {**1**(tol)$_2$}, minor conformer (8.6%). Rotation position: 128°. **C**: {**1**(CNPT)$_2$}, major conformer (78%). Rotation position: 62°. **D**: {**1**}. Rotation position: 90°. The rotation position is defined by the torsion angle N-C-C$^F$-C$^{F6}$, where C$^F$-C$^{F6}$ is the bond joining two six-membered rings, and C$^F$ is the atom attaching the fullerene to the imidazolium fragment. View as in Figure 2A in the main text (imidazolium in the foreground).

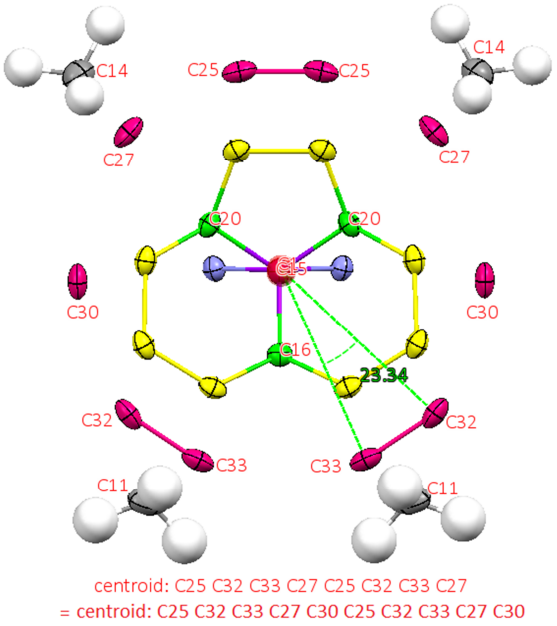


**Figure S4.** Selected atoms in the 80 K structure of {**1**}, illustrating atoms with close intra- and intermolecular contacts. Ellipsoids at 60% probability; most atom labels omitted for clarity. View down the rotation axis from C15 to C1 (imidazolium in the background); C1, C15, and C16 are located on the mirror plane. C1 is bonded to the two (blue) N atoms in the stator. Other colors, as in Figure 3, main text, represent perpendicular (radial) distance from the rotation axis. (The green, yellow, and red fullerene C atoms are also at increasing distances from the stator. See main text.) C11 and C14 are the two independent methyl groups closest to the rotator. The centroid of eight or ten "red" atoms (0.071, 0.25, 0.402 or 0.073, 0.25, 0.407) is marked by a red sphere on the rotation axis. Angle made by bonded atoms at the "red" distance from the rotation axis: C32···centroid···C33 = 23°. (The libration amplitude of about 30(°)$^2$ at 300 K suggests an oscillation of ± 5°, or nearly half a bond length for the atoms most distant from the rotation axis; see Figure S8.)

**Structure quality: Anisotropic Displacement Parameters**

The orientations of atomic displacement parameter (ADP) ellipsoids for bonded atoms (known as the Hirshfeld test) are similar when the ADPs originate from the motion of a given molecular fragment. The ADPs for the solvated ({**1**(tol)$_2$}) and solvent-free ({**1**}) crystals give similar ellipsoid orientations at 100-130 K (Figure S5).

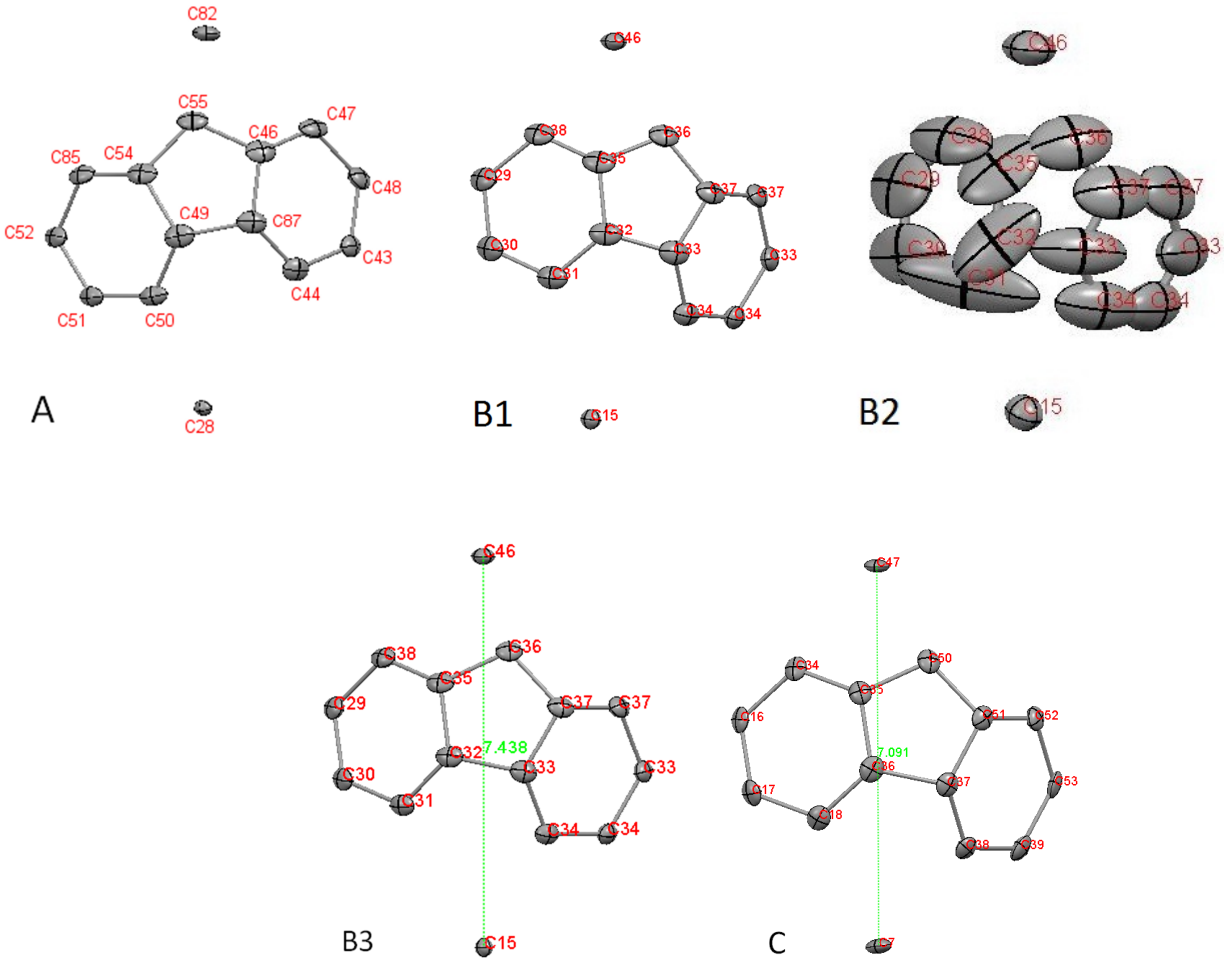


**Figure S5**. **A:** Selected (13) atoms in the maximum-rotation equatorial area of the $C_{60}$ rotator, plus the two axial $C^F$ atoms, from {**1**$(tol)_2$} (major conformer, 91.4%), at 100 K. **B1**, **B2**, and **B3:** A similar fragment from the solvent-free adduct {**1**} at 130 K, 480 K, and 80 K. **C:** A similar fragment from a co-crystal of unsubstituted $C_{60}$ with $C_9Cl_9N$ ($C_9Cl_9N$: perchloroazatriquinacene; 90 K).[ii] All ellipsoids drawn at 50% probability. (Drawings and distances for this and other figures: CSD Mercury.[iii] Atom numbering: In crystals of {**1**}, **1** lies on a mirror plane in space group *Pnma*. C33, C34, and C37 and the mirror-related counterparts appear in **B1**, **B2**, and **B3**.)

In {**1**$(tol)_2$}, bonded atoms C46 and C47 give a Hirshfeld difference of 7.1 su at 100 K. A difference in orientation of the ADP axes is visible in Figure S5A. Principal axis orientations for {**1**} are consistent with rotational motion of $C_{60}$ about the C15···C46 axis up to about 280 K (largest Hirshfeld test 7.0 su). At high temperatures, {**1**} gives many Hirshfeld violations (Figure S2); for example C31-C32 (17.5 su), in Figure S5B2. This is a strong indication of positional disorder and high error in atomic positions.

Figure S5C shows the unsubstituted $C_{60}$ molecule in the co-crystal with perchloroazatriquinacene ($C_9Cl_9N$) at 90 K. Comparing C and B3 in Figure S5 one notes that the ADP ellipsoids are of similar size, but the principal axes have different orientations. Again, those in Figure S5B3 suggest rotation about the vertical axis (length about 7.4 Å) even at 80 K. $C_{60}$ in {$C_{60}(C_9Cl_9N)$}, in contrast, is almost spherical (diameter about 7.1 Å) with nearly equal libration amplitudes along all three inertial axes.

The refinement agreement factors *R*1, w*R*2 (all data) and GOF (0.042-0.049, 0.11-0.14, 1.00-1.05, respectively, from 80 to 280 K) for {**1**} indicate high quality crystal structures. In the sections below we report the results of the analysis of ADPs for {**1**} using the program THMA14C[iv].

**Contacts and symmetry**

The $C_{60}$ portion of {**1**} makes two types of close contacts with its neighbors. Intermolecular contacts include π···π contacts of 3.2-3.4 Å and C-H···π contacts of 2.8-2.9 Å. In addition, the intramolecular C-H···π contacts, C11-H11A···C17 of 2.58 Å (2.47 Å if the C-H distance is lengthened[v]) are shorter than any intermolecular C-H···C distances (see Figure S6 and Table S3).

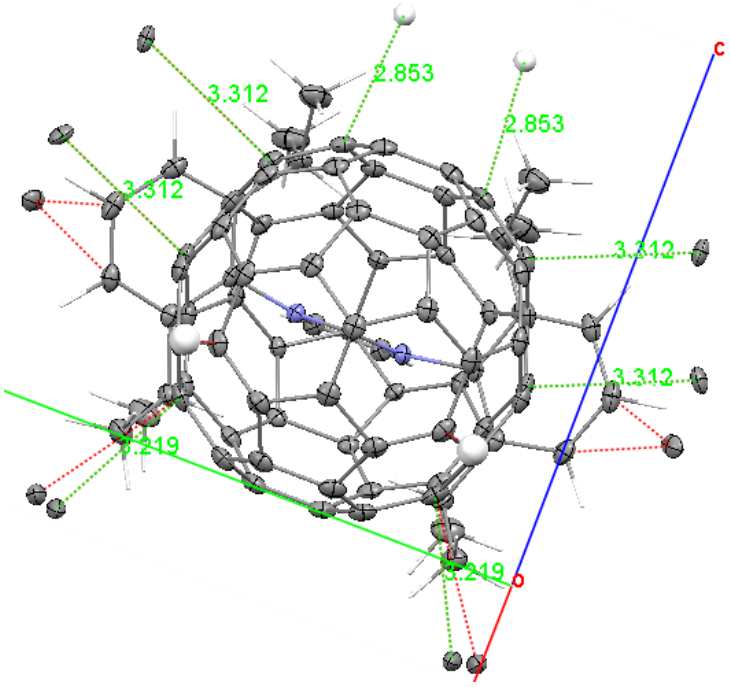


**Figure S6A**. Close intermolecular contacts in the 80 K crystal structure of {**1**}. View down the rotation axis (C46-C15-C1 vector, *cf.* Figure S6B) showing the directions of close contacts listed in Table S3 (below). The mirror plane is parallel to the *a*-*c* plane. The figure shows clearly that there is no 2-fold symmetry about the rotation axis.

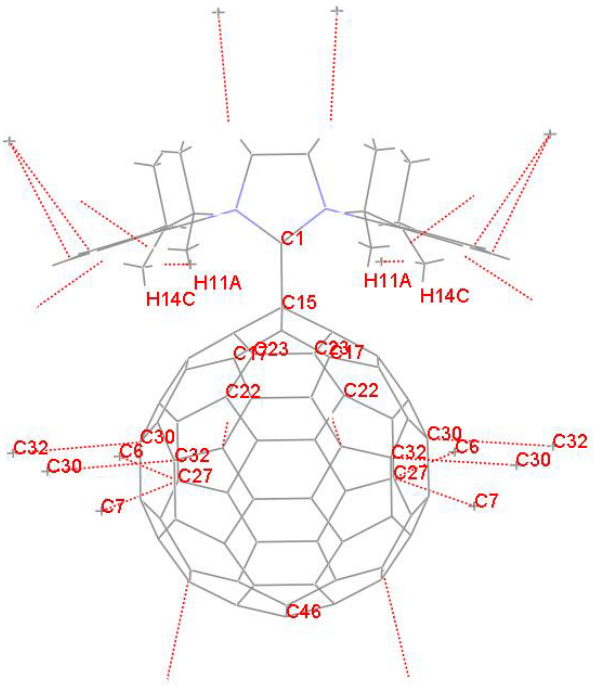


**Figure S6B**. View showing intermolecular contacts; rotation axis vertical. Carbon, hydrogen and nitrogen atoms numbered 1 through 14 are in the carbene moiety, and carbon atoms 15 through 46 are in $C_{60}$. For distances, see Table S3.

**Table S3**. Intermolecular and intramolecular contacts for {**1**} at 80 K as obtained from CSD Mercury.[iii]

| Contact | Atom1 | Atom2 | Symm. op. 1 | Symm. op. 2 | Length/Å | Length-VdW |
|---|---|---|---|---|---|---|
| 1 | C27 | C7 | x,y,z | 1/2-x,-y,-1/2+z | 3.389 | -0.011 |
| 2 | C27 | C6 | x,y,z | 1/2-x,-y,-1/2+z | 3.219 | -0.181 |
| 3 | H14A | H11C | x,y,z | 1/2-x,-y,-1/2+z | 2.361 | -0.039 |
| 13 | C32 | C30 | x,y,z | -x,-y,1-z | 3.312 | -0.088 |
| 17 | C42 | H14B | x,y,z | -1/2+x,y,1/2-z | 2.811 | -0.089 |
| 19 | C33 | H2 | x,y,z | -1/2+x,y,1.5-z | 2.853 | -0.047 |
| Intramolecular | Atom1 | Atom2 | | | Length/Å | |
| 1 | N1 | C20 | x,y,z | x,y,z | 3.055(2) | -0.195 |
| 2 | N1 | C16 | x,y,z | x,y,z | 3.427(2) | 0.177 |
| 3 | C23 | C14 | x,y,z | x,y,z | 3.633(2) | 0.233 |
| 4 | C17 | C11 | x,y,z | x,y,z | 3.436(2) | 0.036 |
| 5 | C23 | H14C | x,y,z | x,y,z | 2.993(1) | 0.093 |
| 6 | C20 | C12 | x,y,z | x,y,z | 3.423(2) | 0.023 |
| 7 | C16 | C9 | x,y,z | x,y,z | 3.723(2) | 0.323 |
| 8 | C20 | C8 | x,y,z | x,y,z | 3.187 | -0.213 |
| 9 | C19 | C3 | x,y,z | x,y,z | 3.201 | -0.199 |
| 10 | C19 | C8 | x,y,z | x,y,z | 3.238 | -0.162 |
| 11 | C18 | C4 | x,y,z | x,y,z | 3.399 | -0.001 |
| 12 | C17 | H11A | x,y,z | x,y,z | 2.582 | -0.318 |

The intramolecular $C^{F}\cdots C^{C}$ (fullerene to imidazolium) non-bonded distances will change under axial rotation of $C_{60}$ with respect to the imidazolium. The closest fullerene atoms to N1 are C16, C20, and C20', with bond angles of 99° (C20-C15-C20') and 110° (C20-C15-C16), giving an approximate 3-fold rotational symmetry (Figures S4 and S7A). Figure S4 and Figure 3A, main text, show the increase in ADP principal axis lengths for $C_{60}$ as distance from the rotation axis increases. Figure S7B shows the effect of a 180° rotation of the $C_{60}$ moiety on some intramolecular contacts. Figure S7C includes views of intermolecular contacts.

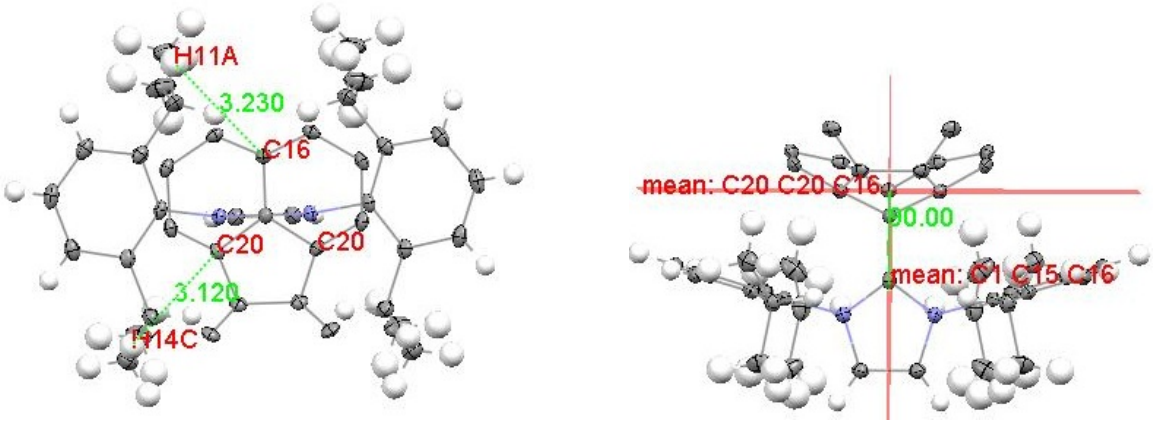


**Figure S7A**. The fullerene atoms closest to N1: C16, C20, and C20'. Left: Looking down the rotation axis. Right: Small portion of the fullerene; the C16, C20, C20' plane is perpendicular to the rotation axis; N1 is 2.94 Å below this plane.

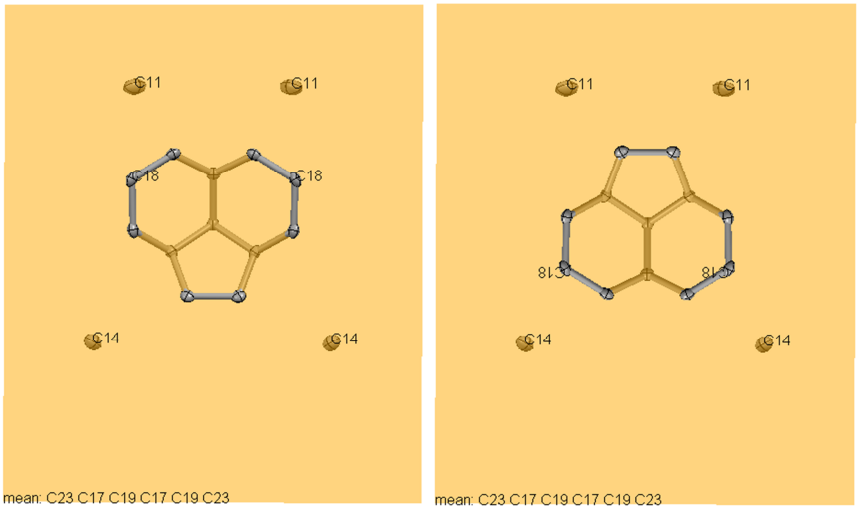


**Figure S7B.** Looking down on the plane C23-C17-C19-C17'-C19'-C23' before and after a 180° rotation of the fullerene moiety. C18 is 0.26 Å above this plane.

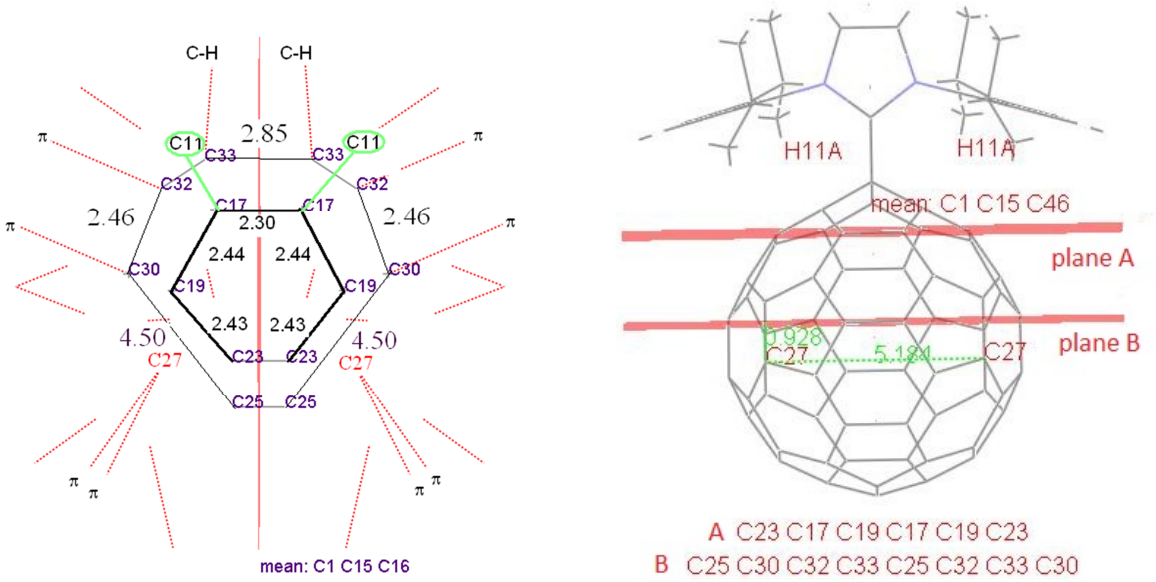


**Figure S7C**. Left: View down the rotation axis showing locations of atoms in a roughly 6- or-8-membered "ring" (intramolecular contacts, plane A; see also Figures S4 and S7B) and an 8- or 10-membered "ring" of intermolecular contacts, plane B. Right: The nearly-parallel mean planes of these atoms, perpendicular to the rotation axis. C27 lies 0.9 Å below plane B. The orientations are similar to those in Figure S6.

To estimate the barrier to rotation of the $C_{60}$ moiety, we may use the cosine function $V = (B/2)(1-\cos n\phi)$[vi], for which $\langle\phi^2\rangle$ is the mean square libration amplitude calculated from the refined U values (ADPs). We can choose n, the symmetry of rotation, from the approximate symmetry of the intramolecular and intermolecular contacts (see Figures S7A, S7B, and S7C).

**Thermal motion analysis with THMA14C**

Thermal motion analysis (THMA14C[iv,vii]) shows that the $C_{60}$ portion of the molecule rotates with respect to the imidazolium portion. Typical results follow. For the solvent-containing structure {**1**$(tol)_2$} at 100 K, the principal axis of libration is also along the C1-fullerene axis, but the agreement factors are not as good as those for the solvent-free molecule.

80 K
Whole molecule {**1**}
EIGENVECTORS AND EIGENVALUES OF L AND T IN THE INERTIAL-FRAME

| L-TENSOR | XI(1) | XI(2) | XI(3) | VALUE(I) | RMS (RAD.) | VALUE(I) (DEG. SQ.) | RMS (DEG.) | |
|---|---|---|---|---|---|---|---|---|
| VEC(1) | 0.99101 | 0.00000 | -0.13377 | 0.00116 | 0.0340 | 3.80 | 1.95 | L1 |
| VEC(2) | 0.00000 | 1.00000 | 0.00000 | 0.00030 | 0.0173 | 0.98 | 0.99 | L2 |
| VEC(3) | 0.13377 | 0.00000 | 0.99101 | 0.00022 | 0.0147 | 0.71 | 0.84 | L3 |

Hirshfeld test: R.M.S. DIFF = 0.0013, bonded; MEAN STANDARD DEVIATION OF U OBSERVED: 0.0007
WEIGHTED R FOR ALL U'S = 0.238; FOR DIAGONAL U'S ONLY, WEIGHTED R = 0.172; Goodness of fit = 4.85

$C_{60}$ plus C1 (33 atoms, 5 on mirror, so total is 33 + 28 generated by mirror = 61)
EIGENVECTORS AND EIGENVALUES OF L AND T IN THE INERTIAL-FRAME

| L-TENSOR | XI(1) | XI(2) | XI(3) | VALUE(I) | RMS (RAD.) | VALUE(I) (DEG. SQ.) | RMS (DEG.) | |
|---|---|---|---|---|---|---|---|---|
| VEC(1) | 0.99509 | 0.09900 | 0.00000 | 0.00161 | 0.0401 | 5.27 | 2.30 | L1 |
| VEC(2) | 0.00000 | 0.00000 | -1.00000 | 0.00051 | 0.0226 | 1.68 | 1.30 | L2 |
| VEC(3) | -0.09900 | 0.99509 | 0.00000 | 0.00048 | 0.0219 | 1.58 | 1.26 | L3 |

Hirshfeld test: R.M.S. DIFF = 0.0012, bonded; MEAN STANDARD DEVIATION OF U OBSERVED: 0.0007
WEIGHTED R FOR ALL U'S = 0.087; FOR DIAGONAL U'S ONLY, R = 0.062; Goodness of fit = 1.69
Coordinates of C1, C15, and C46 in the I-frame: C1 , -5.22244 -0.50898 0.00000; C15, -3.69875 -0.34294 0.00000; C46, 3.70808 0.33618 0.00000. Therefore the C1 to C15 to C46 vector is close to the X axis in the I-frame. (8.9 Å along X, 0.8 Å along Y, 0.0 along Z; actual distance C1···C46 = 8.97 Å).

100 K

{**1**(tol)$_2$}, $C_{60}$ plus C1 before minor conformer introduced

EIGENVECTORS AND EIGENVALUES OF L AND T IN THE I-FRAME

| L-TENSOR | XI(1) | XI(2) | XI(3) | VALUE(I) | RMS (RAD.) | VALUE(I) (DEG. SQ.) | RMS (DEG.) | |
|---|---|---|---|---|---|---|---|---|
| VEC(1) | 0.99137 | -0.13023 | 0.01531 | 0.00245 | 0.0495 | 8.05 | 2.84 | L1 |
| VEC(2) | -0.01782 | -0.24951 | -0.96821 | 0.00076 | 0.0276 | 2.49 | 1.58 | L2 |
| VEC(3) | 0.12991 | 0.95958 | -0.24968 | 0.00065 | 0.0256 | 2.14 | 1.46 | L3 |

Hirshfeld test: R.M.S. DIFF = 0.0025, bonded; MEAN STANDARD DEVIATION OF U OBSERVED: 0.0008

Hirshfeld differences: C56-C77, -58; C56-C57, -75

WEIGHTED R FOR ALL U'S = 0.157; FOR DIAGONAL U'S ONLY, WEIGHTED R = 0.119; Goodness of fit = 3.26

Coordinates of C1, C28, and C82 in the I-frame: C1, -5.31097 0.03284 0.01384; C28, -3.78407 0.01993 0.00692; C82, 3.63253 -0.02541 -0.01210; C28···C82 = 7.417 Å; C1···C82 = 8.944 Å.

{**1**(tol)$_2$}, C1 + C28-C87, major conformer (91.4%)

EIGENVECTORS AND EIGENVALUES OF L AND T IN THE I-FRAME

| L-TENSOR | XI(1) | XI(2) | XI(3) | VALUE(I) | RMS (RAD.) | VALUE(I) (DEG. SQ.) | RMS (DEG.) | |
|---|---|---|---|---|---|---|---|---|
| VEC(1) | 0.99175 | -0.10657 | 0.07129 | 0.00212 | 0.0460 | 6.95 | 2.64 | L1 |
| VEC(2) | 0.08815 | 0.97050 | 0.22440 | 0.00072 | 0.0268 | 2.36 | 1.54 | L2 |
| VEC(3) | -0.09310 | -0.21627 | 0.97189 | 0.00060 | 0.0245 | 1.97 | 1.41 | L3 |

Hirshfeld test: R.M.S. DIFF = 0.0019, bonded; MEAN STANDARD DEVIATION OF U OBSERVED: 0.0006

Hirshfeld difference: C46-C47, 78

WEIGHTED R FOR ALL U'S = 0.118; FOR DIAGONAL U'S ONLY, WEIGHTED R = 0.092; Goodness of fit = 2.60

For {**1**}, the amplitude of libration of $C_{60}$ about the C1-C15-C46 axis (L1) is about 5.3(°)$^2$ while L1 in the same direction for the entire molecule is smaller, about 3.8(°)$^2$. (L1 for the $C_{60}$ + C1 fragment is thus $\langle\phi^2\rangle$ in a torsional model for the rotational potential.[viii]) The motion of the fragment is greater than that of the molecule as a whole, and the agreement factors (Hirshfeld test[i] (RMSΔ), R(diag) and GOF) for the fragment are also better.

For the solvate {**1**(tol)$_2$} at 100 K, L1 is also greatest about the same inertial axis. The agreement factors are improved by introduction of the minor conformer, and the magnitude of L1 (7.0(°)$^2$) is comparable to that of the solvent-free rotator, yet the Hirshfeld tests are not as good (Figure S5A).

In contrast, the unsubstituted $C_{60}$ in a co-crystal with $C_9Cl_9N$[ii] (from a crystal structure of very high quality at approximately the same temperature, see Figure S5C) gives similar libration amplitudes along all three inertial axes, also with excellent agreement factors.

90 K

$C_{60}$ in {$C_{60}(C_9Cl_9N)$}[ii] (60 atoms; Figure S5C)

EIGENVECTORS AND EIGENVALUES OF L AND T IN THE I-FRAME

| L-TENSOR | XI(1) | XI(2) | XI(3) | VALUE(I) | RMS (RAD.) | VALUE(I) (DEG. SQ.) | RMS (DEG.) | |
|---|---|---|---|---|---|---|---|---|
| VEC(1) | -0.62756 | -0.26474 | -0.73218 | 0.00140 | 0.0374 | 4.60 | 2.15 | L1 |
| VEC(2) | -0.32053 | -0.76917 | 0.55285 | 0.00113 | 0.0336 | 3.71 | 1.93 | L2 |
| VEC(3) | -0.70953 | 0.58162 | 0.39784 | 0.00107 | 0.0327 | 3.50 | 1.87 | L3 |

Hirshfeld test: R.M.S. DIFF = 0.0016, bonded; MEAN STANDARD DEVIATION OF U OBSERVED: 0.0012

WEIGHTED R FOR ALL U'S = 0.095; FOR DIAGONAL U'S ONLY, WEIGHTED R = 0.069; Goodness of fit = 0.98

**Table S4.** Summary of Thermal Motion Analysis Results for the Entire Molecule and for the Rotator in Crystals {**1**} from 80-480 K.

| T/K | NHC-$C_{60}$ L1[a] (molec) | $C_{60}$+C1 L1[a] (rotator) | GOF (molec) | GOF (rotator) | R(diag) (rotator) | RMSΔ×$10^3$ (fragment) (Hirshfeld[i] test) | MESDU×$10^3$ (molec) | MESDU×$10^3$ (rotator) | No. of Hirshfeld violations[1] |
|---|---|---|---|---|---|---|---|---|---|
| 80 | 3.80 | 5.27 | 4.85 | 1.69 | 0.062 | 12 | 7 | 7 | 0 |
| 130 | 6.06 | 8.39 | 5.83 | 1.83 | 0.054 | 13 | 7 | 7 | 0 |
| 180 | 8.64 | 12.44 | 7.12 | 2.24 | 0.056 | 16 | 8 | 8 | 0 |
| 230 | 11.89 | 18.06 | 8.22 | 2.68 | 0.063 | 20 | 9 | 9 | 0 |
| 280 | 15.26 | 25.59 | 8.89 | 3.54 | 0.087 | 44 | 12 | 12 | 5 |
| 330 | 18.39 | 36.17 | 8.74 | 4.23 | 0.122 | 94 | 19 | 19 | 7 |
| 380 | 21.70 | 51.88 | 8.10 | 4.58 | 0.164 | 202 | 32 | 34 | 9 |
| 430 | 24.62 | 77.01 | 8.02 | 4.95 | 0.199 | 367 | 51 | 56 | 20 |
| 480 | 27.11 | 104.22 | 7.65 | 5.48 | 0.260 | 905 | 93 | 107 | 34 |

[a]L1 (<$\phi^2$>) is the libration amplitude about the C1-C15···C46 axis.

It is evident in Table S4 that the libration amplitude about the C1-C15···C46 axis is greater at all temperatures for the $C_{60}$ + C1 rotator than for the entire molecule. Above *ca*. 280 K, order in the structure deteriorates rapidly, as seen by agreement factors GOF and R, and by the increase in MESDU (mean su, or mesd(U)). As suggested by the orientation of the ellipsoids for the 480 K structure in Figure S5B2, and the Hirshfeld test violations (Figure S2 and Table S4), the U values at higher temperatures no longer describe rigid-body motion.

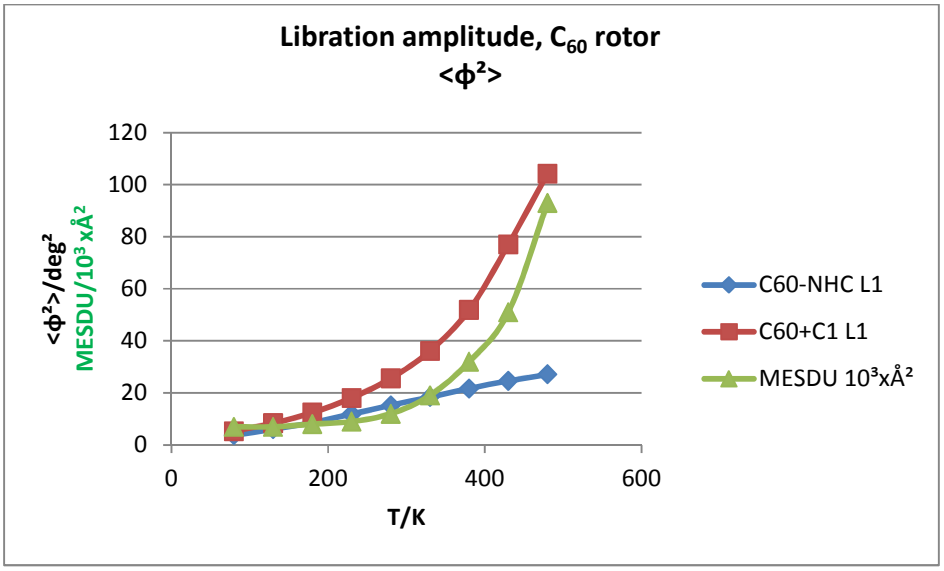


**Figure S8**. Libration amplitude as a function of temperature. <$\phi^2$> vs. T: blue curve, NHC-$C_{60}$ adduct; red curve, $C_{60}$ + C1 rotor as an isolated molecule. The green curve shows the increase in mesd(U) (entire molecule, Table S4) with T.

Because the methyl groups in the isopropyl moieties of **1** vary in bond lengths and in ADP magnitudes, the molecule as a whole was also treated as a rigid body with a) four Me attached rigid groups (ARGs) or b) two *i*-Pr ARGs. Table S5 presents some features of model b, for three temperatures.

**Table S5.** Summary of Thermal Motion Analysis results for {**1**} with two isopropyl groups as ARGs.

| T/K | {**1**} L1 molecule | GOF molecule | R(diag) | <$\phi^2$>, C9-C10, C11 | <$\phi^2$>, C12-C13, C14 | Bond C9-C11 | Bond C12-C14 | Bond Correction C9-C11 | Bond Correction C12-C14 |
|---|---|---|---|---|---|---|---|---|---|
| 80 | 3.8 | 4.7 | 0.15 | 9 (6) | 20 (5) | 1.525(2) | 1.529(2) | 0.003 | 0.010 |
| 130 | 6.0 | 5.6 | 0.15 | 16 (8) | 29 (7) | 1.526(2) | 1.528(2) | 0.004 | 0.007 |
| 280 | 15.2 | 8.8 | 0.20 | 42 (25) | 52 (21) | 1.525(4) | 1.523(3) | 0.011 | 0.013 |

[1] checkCIF/Platon report

Overall libration amplitudes and agreement factors are unchanged by including the isopropyl groups (or methyl groups) as ARGs (NHC-$C_{60}$ L1, molecule, Table S5). At all three temperatures, the libration amplitude ($<\phi^2>$) of the isopropyl group C12-C13, C14 is larger than that of C9-C10, C11. We presume the motion of C11 is restricted by the close intramolecular C-H···C contact, C11-H11A···C17 of 2.58 Å (Table S3). The larger the libration amplitude, the larger the bond length correction due to thermal motion. Bond length corrections are of the order of 2-4 mesd. At 80 K, the correction for C13-C14 is more than 3 times that for C9-C11. As temperature increases, $<\phi^2>$ values and bond length corrections for the two isopropyl groups become more nearly equal.

**Suggested barriers to rotation**

THMA14C-calculated amplitudes of libration for the $C_{60}$ + C1 rotor are small (about $30(°)^2$ at 300 K) and imprecise at higher temperatures. The rotation symmetry in the crystal is Cs (m), but intra- and intermolecular contacts suggest additional minima (Figures S6 and S7). The approximate symmetry of the contacts is 3-fold (intramolecular, Figure S7A), 6- or 8-fold (intramolecular, Figures S7B, S7C), and 8- or 10-fold (intermolecular, Figure S7C).

Calculations (PM6, Figure 5C, main article) for {**1**} in the crystal surroundings give minima at about 45, 90, 135, 195, 240, 270, 300, and 345°, suggesting an approximately 8-fold potential.

Barriers only calculated in THMA14C for "attached rigid groups" (ARGs, such as the isopropyl groups in Table S5). The rotator contains too many atoms to be treated as an ARG, but barriers may be estimated by considering the rotator as an independent molecule with L1 = $<\phi^2>$, corresponding to the sinusoidal potential $V = B/2(1-\cos n\phi)$.[vi,viii] The barrier is then calculated from the relation between RT/B and $<\phi^2>$ for the desired value of n. At low values of $<\phi^2>$, the harmonic approximation for the barrier may also be used.[ix] For $<\phi^2> = 30(°)^2$ at 300 K, the barriers for n = 3, 6, 8, and 10 are about 14, 4.3, 2.4, and 1.4 kcal/mol, respectively[2] (Figure S9A).

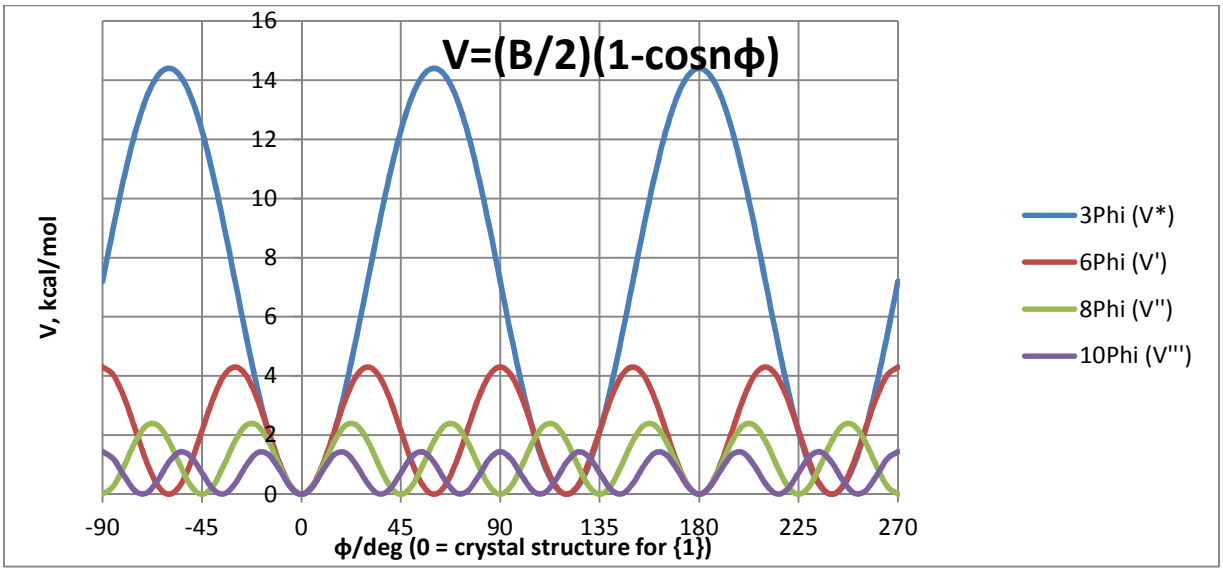


**Figure S9A**. Cosine functions at 300 K for 3-fold (blue), 6-fold (red), 8-fold (green) and 10-fold (purple) potentials. The libration amplitude $<\phi^2>$ is $30(°)^2$ for each curve (see text). $\phi$ = 0° represents a 90° rotation for Figure 5 in the main text.

We note here that a 6-fold rotational barrier for unsubstituted $C_{60}$ of 36.4 kJ/mol (8.7 kcal/mol) was calculated from L1 = $<\phi^2> = 8.3(°)^2$ at 200 K.[x] For comparison, L1 = $<\phi^2>$ for the $C_{60}$ + C1 rotor would be about $15(°)^2$ at 200 K for {**1**} (Table S4).

[2] Barriers were estimated with the torsional model for n = 3 and n = 6. The harmonic approximation (B is inversely proportional to $n^2$) was used to calculate barriers for n = 8 and n = 10. Values at 280 K are 20, 5.0, 2.8, and 1.8 (based on torsional model for n = 6).

Figure S9A shows minima for the 8-fold potential (green curve) at 0°, 45°, 90°, 135°, and 180°, corresponding to 90°, 135°, 180°, 225° and 270° in Figure 5 (main text). In the PM6 calculations, intramolecular interactions have been suppressed, since the molecule is allowed to relax after each rotational increment. Only the crystal surroundings remain fixed. For this reason we expect small contributions from intramolecular (3-fold and 6-fold) potentials. Figure S9B shows a trial combination of 80% 8-fold (intermolecular), 18% 6-fold and 2% 3-fold (both intramolecular) contributions. Slight displacement of minima positions and barrier heights of about 2-3 kcal/mol are the result of this combination of sinusoidal functions.

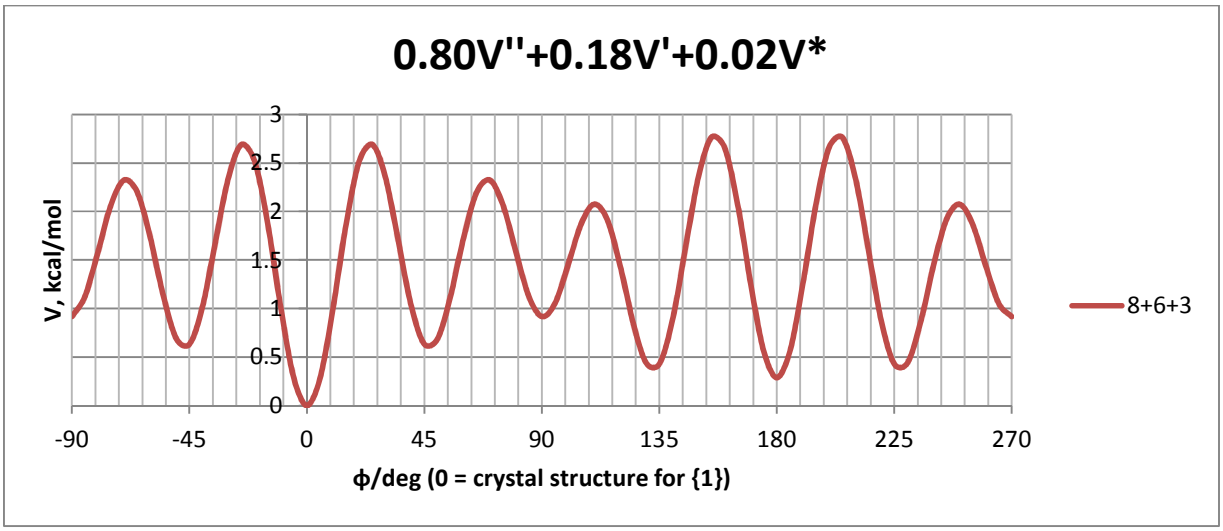


**Figure S9B**. A trial function resulting from a combination of the 8-, 6- and 3-fold sinusoidal potentials shown in Figure S9A.

Figure S9B is an approximation, because $\langle\phi^2\rangle = 30(°)^2$, the libration amplitude at 300 K and the 3-, 6-, 8-, and 10-fold symmetries corresponding to Figures S6 and S7 are approximate; the choice of the trial function is arbitrary. Still, the summary curve does suggest a range of barriers estimated from ADPs and atom-atom contacts in the crystal, as well as possible locations of subsidiary minima and maxima for comparison with more precise calculations.

**Conclusions from Thermal motion analysis of solvent-free {1}**

Treating the $C_{60}$ + C1 moiety in {**1**} as a rigid body for thermal motion analysis gives an excellent fit to rotation about the axis of attachment to the imidazolium portion of the molecule, from 80 K to 280 K. However, the amplitude of libration is small, about $30(°)^2$ at 300 K, indicating either a high barrier to rotation, or a large number of minima per revolution. Semiempirical calculations with the PM6 potential revealed eight energy minima and eight energy maxima with relatively low barriers in the crystal (Figure 5 in the main article). Analysis of the ADPs indicates that above room temperature there is positional as well as motional disorder, which also supports low barriers and several minima. At higher temperatures some of the additional low-energy states are probably occupied.

## Computational Studies of 1

### Isolated molecule calculations

The optimization of the structure for isolated **1** was performed using DFT and semiempirical methods. For the semiempirical methods AM1,[xi] PM3,[xii] and PM6[xiii] were used. For the DFT based calculations, B3LYP,[xiv] B97D,[xv] and M06-2X[xvi] functionals were used with a 6-31G(d,p) basis set.

The scan around the C1-C15 bond was performed using the GAUSSIAN program.[xvii] The dihedral angle N1-C1-C15-C16 was chosen as the scan coordinate (Figure S10), which was kept frozen while relaxing all other coordinates. To construct the energy curve, 20 points for the dihedral angle were calculated from 0° to 90°. The full 360° curve was obtained using the system symmetry.

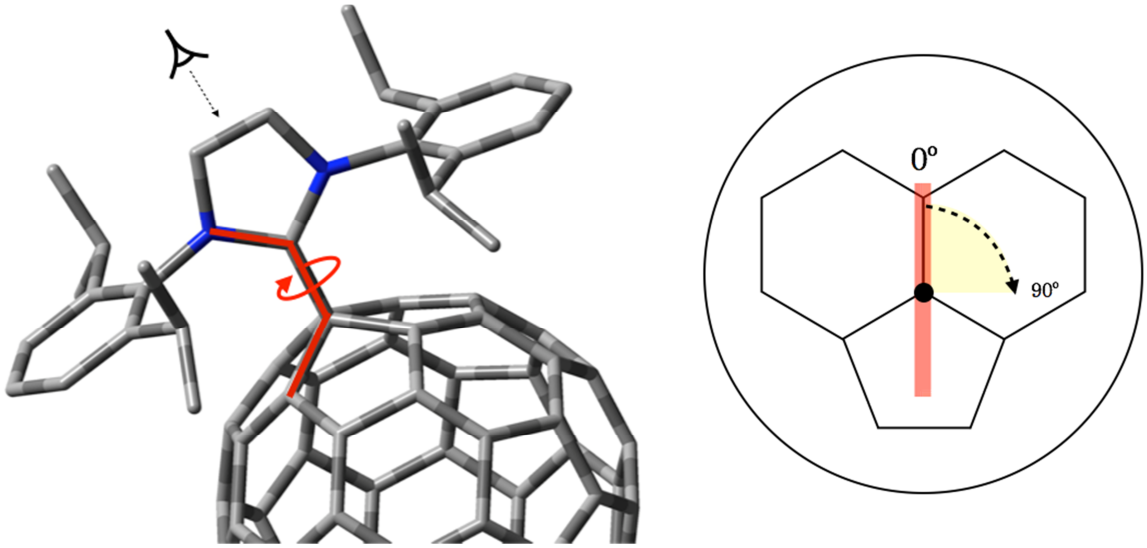


**Figure S10**. Dihedral scanning coordinate.

### Energy profiles for isolated 1 obtained with DFT methods

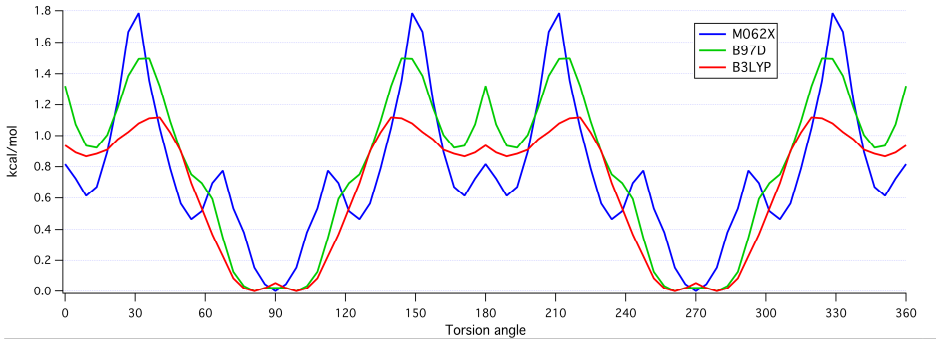


**Figure S11**. Energy profile along the rotation around the C1-C15 bond for the single molecule using DFT methods.

The DFT energy profiles for rotation along the C1-C15 bond are shown in Figure S11. For all methods, we obtain a low rotational barrier of less than 2 kcal/mol, indicating that there are no strong intramolecular interactions and that rotation of the $C_{60}$ fragment around the C1-C15 axis should be facile at room temperature. For all three DFT based methods we obtain a qualitatively similar curve with the absolute minimum at 90°, a maximum around 30°-40° and, in B3LYP and B97D, a shallow local minimum at 0°/180°. The heights of the barriers relative to the 90° minimum energy

structure are 1.11 kcal/mol (B3LYP), 1.59 kcal/mol (B97D), and 1.79 kcal/mol (M06-2X). The barriers around the 0° local minimum are 0.22 kcal/mol (B3LYP) and 0.15 kcal/mol (B97D). As a difference between the B3LYP and the other two functionals we can see that for the latter there is a local maximum (M06-2X) or a shoulder (B97D) in the region around 50°. Although there are also small maxima at 90° and 180°, these may be an artifact due to the finite precision used in the geometrical optimization process.

**Table S6.** Absolute energies of the lowest energy rotamers for isolated **1** obtained with DFT methods.

| DFT functionals | Minimum Energy (Hartree) |
|---|---|
| B3LYP | -3446.26367405 |
| B97D | -3443.75456737 |
| M06-2X | -3445.06252352 |

**Energy profiles for isolated 1 obtained with semiempirical methods**

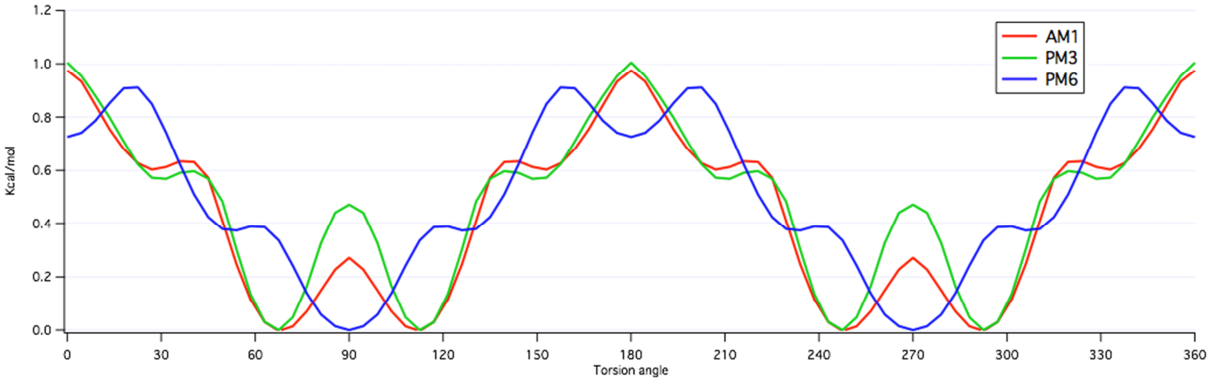


**Figure S12**. Energy profile along the rotation around the C1-C15 axis for the single molecule using semiempirical methods.

The calculated barriers for **1** using semiempirical methods are somewhat lower than those obtained with DFT based methods: 0.97 kcal/mol (AM1), 1.00 kcal/mol (PM3), and 0.91 kcal/mol (PM6). Although these energy differences are not quantitatively reliable, we get the same qualitative answer as in the DFT calculations: the rotation of $C_{60}$ should be facile in the absence of strong intermolecular interactions in the crystal.

Among the semiempirical methods however, only PM6 seems to describe correctly the qualitative behavior of the potential energy curves calculated at the DFT level. The minimum energy conformation at 90° and the two maxima between 135°-225° shown by DFT for all three functionals are only correctly reproduced in the curve calculated using the PM6 method. Both for AM1 and PM3 the 90° and 0°/180° geometries correspond to maxima in the curve and two symmetric absolute minima at 67° and 113° are found using the two methods.

**Table S7.** Absolute energies of the lowest energy rotamers for isolated **1** obtained with semiempirical methods.

| Semiempirical methods | Minimum (Hartree) |
|---|---|
| AM1 | 1.66563443 |
| PM3 | 1.33044530 |
| PM6 | 1.29297143 |

**Cluster calculations**

The calculation of **1** inside the crystal environment was performed with PM6 semiempirical method.

The crystal environment was constructed by taking the nearest neighbors of a single molecule **1** in the solvent free crystal structure {**1**} at 100 K, including all atoms within a radius of about 5 Å from the molecule surface. The "broken" fragments representing the environment were saturated with hydrogen atoms as shown in Figure S13.

For the scan around the C1-C15 bond, the same scan coordinate described for single molecule calculations were used. The crystal environment atoms were frozen during the scan, while the whole main molecule was relaxed (except for the dihedral angle N1-C1-C15-C16).

Due to the lower symmetry of the cluster, as compared to that of the single molecule, the scan around the C1-C15 bond was performed from 90° to 270° using 40 data points (Figure S14). The full 360˚ curve was constructed using the mirror symmetry of the structure in {**1**}.

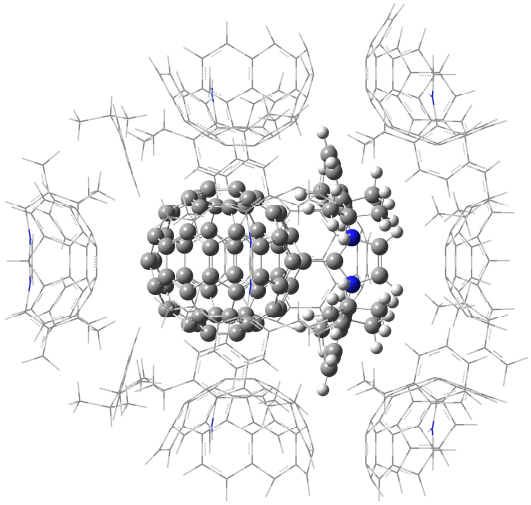

**Figure S13**. Cluster model used to study the rotation of the fullerene moiety in **1** embedded in its crystal environment.

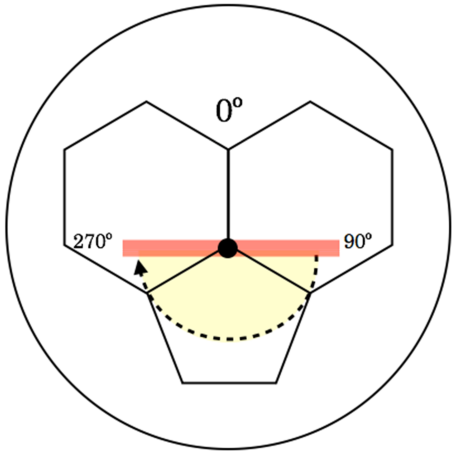


**Figure S14**. Scan coordinate for the cluster calculation.

**Energy profiles for single molecule and cluster calculations using PM6 method**

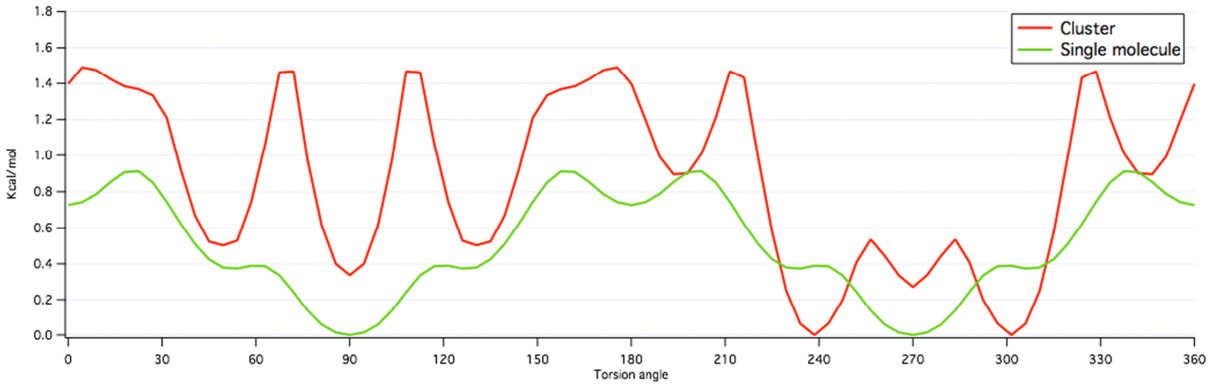


**Figure S15**. Energy profile along the rotation around the C1-C15 bond using PM6 method for single molecule and cluster calculations.

Figure S15 shows a comparison between the potential energy of the molecule embedded in the crystal and the molecule with the same geometry but without the crystal environment. The difference between the two curves illustrates distortion effects caused by the environment. For example, it can be seen that the intermediate barrier at 66° increases its value in the cluster with respect to that in the free molecule, suggesting unfavorable intermolecular steric and/or electronic forces within the crystal.

In conclusion, we can appreciate a slight increase of the potential energy barrier from ca. 1.00 to 1.14 kcal/mol from the isolated molecule to the cluster, which should not have a significant influence at room temperature. However, it is significant that the potential has a relatively large number of energy minima and maxima that are relatively narrow. We hypothesize that these narrow features are responsible for the small librational amplitude $\langle\phi^2\rangle$ observed at low temperatures, and for the rapid departure of the $\langle\phi^2\rangle$ values from an expected $T^{3/2}$ dependence, which was observed at higher temperatures. These results are qualitatively consistent with the evidence of occupational disorder that occurs at temperatures above 280 K.

**Table S8.** Structural parameters calculated for the adduct **1** and the two separated fragments **$Ar_2$NHC** and $C_{60}$ in the gas phase. Data in the last column correspond to the calculation of adduct **1** embedded in a model for the cavity created by its nearest neighbors in the crystal structure. Distances are given in Å, angles in (˚). The labels used to identify individual C atoms are the same as in Figure 1, main text. Experimental data were determined at *T* = 100 K.

| Structural parameter | Method | **$Ar_2$NHC** | $C_{60}$ | **$Ar_2$NHC**-$C_{60}$ | **$Ar_2$NHC**-$C_{60}$ (embedded) |
|---|---|---|---|---|---|
| **$C_{ipso}$-C** (C15-C16, hexagons) | B3LYP | | 1.395 | 1.539 | |
| | B97D | | 1.405 | 1.534 | |
| | M06-2X | - | 1.387 | 1.526 | |
| | PM6 | | 1.386 | 1.499 | 1.501 |
| | **Exp.** | | **1.391** | **1.532** | **1.532** |
| **$C_{ipso}$-C** (C15-C20, hexagon-pentagon) | B3LYP | | 1.453 | 1.561 | |
| | B97D | | 1.456 | 1.560 | |
| | M06-2X | - | 1.451 | 1.554 | |
| | PM6 | | 1.469 | 1.547 | 1.551 |
| | **Exp.** | | **1.455** | **1.557** | **1.557** |
| **average C-C distance within the $C_{60}$ moiety** | B3LYP | | 1.434 | 1.433 | |
| | B97D | | 1.439 | 1.438 | |
| | M06-2X | - | 1.430 | 1.429 | |
| | PM6 | | 1.441 | 1.440 | 1.439 |
| | **Exp.** | | **1.43** | **1.43** | **1.43** |
| **$C_{60}$ diameter** (C15-C45) Value relative to free $C_{60}$ in parenthesis | B3LYP | | 7.100 | 7.438(+0.34) | |
| | B97D | | 7.123 | 7.424(+0.30) | |
| | M06-2X | - | 7.078 | 7.402(+0.32) | |
| | PM6 | | 7.134 | 7.433(+0.30) | 7.450(+0.32) |
| | **Exp.** | | | **7.426(+0.35)** | **7.426(+0.35)** |
| **C-C adduct** C1-C15 | B3LYP | | | 1.541 | |
| | B97D | | | 1.520 | |
| | M06-2X | - | - | 1.525 | |
| | PM6 | | | 1.524 | 1.520 |
| | **Exp.** | | | **1.530** | **1.530** |
| **N-C in $Ar_2$NHC** N-C1 Value relative to free **$Ar_2$NHC** in parenthesis | B3LYP | 1.375 | | 1.364(-0.011) | |
| | B97D | 1.380 | | 1.361(-0.019) | |
| | M06-2X | 1.386 | - | 1.350(-0.036) | |
| | PM6 | 1.391 | | 1.390(-0.001) | 1.391(0.000) |
| | **Exp.** | 1.367 | | **1.352(-0.015)** | **1.352(-0.015)** |
| **N-C-N in $Ar_2$NHC** N-C1-N | B3LYP | 101.5 | | 106.0 | |
| | B97D | 100.9 | | 106.4 | |
| | M06-2X | 101.2 | - | 106.4 | |
| | PM6 | 104.6 | | 106.6 | 106.7 |
| | **Exp.** | **101.4** | | **106.5** | **106.5** |

**Table S9.** Charge separation (in electrons, obtained from a Mulliken analysis) and dipolar moment (Debye) calculated for the adduct **1** in the gas phase.

| Method | Charge separation | $\mu$ |
|---|---|---|
| B3LYP | ± 0.69 | 15.26 |
| B97D | ± 0.69 | 15.22 |
| M06-2X | ± 0.69 | 14.76 |
| PM6 | ± 0.73 | 16.23 |

**Table S10.** Charges in the imidazolium ring (in electrons, obtained from a Mulliken analysis) for free **$Ar_2$NHC**, **$Ar_2$NHC**-$H^+$, and the adduct **1** (**$Ar_2$NHC**-$C_{60}$) in the gas phase. The numbering of the atoms is as in Figure 1, main text.

| | **$Ar_2$NHC** | | | **$Ar_2$NHC**-$H^+$ | | | **$Ar_2$NHC**-$C_{60}$ | | |
|---|---|---|---|---|---|---|---|---|---|
| Method | C1 | N | C2 | C1 | N | C2 | C1 | N | C2 |
| B3LYP | 0.123 | -0.507 | 0.042 | 0.346 | -0.470 | 0.078 | 0.616 | -0.560 | 0.080 |
| B97D | 0.126 | -0.495 | 0.034 | 0.338 | -0.472 | 0.067 | 0.608 | -0.541 | 0.067 |
| M06-2X | 0.177 | -0.545 | 0.018 | 0.342 | -0.507 | 0.053 | 0.623 | -0.567 | 0.053 |
| PM6 | 0.071 | -0.221 | -0.166 | -0.055 | -0.043 | -0.125 | 0.152 | -0.029 | -0.140 |

**Table S11.** Geometry of the imidazolium ring (distances in Å, angles in °) for free **$Ar_2$NHC**, **$Ar_2$NHC**-$H^+$, and the adduct **1** (**$Ar_2$NHC**-$C_{60}$) in the gas phase. The numbering of the atoms is as in Figure 1, main text. Only M06-2X and PM6 results are included for simplicity.

| | **$Ar_2$NHC** | | **$Ar_2$NHC**-$H^+$ | | **$Ar_2$NHC**-$C_{60}$ | |
|---|---|---|---|---|---|---|
| | M06-2X | PM6 | M06-2X | PM6 | M06-2X | PM6 |
| C1-N | 1.368 | 1.391 | 1.332 | 1.383 | 1.350 | 1.389 |
| C2-N | 1.391 | 1.434 | 1.380 | 1.401 | 1.382 | 1.411 |
| C-C | 1.351 | 1.372 | 1.361 | 1.394 | 1.351 | 1.382 |
| N-C1-N | 101.2 | 104.6 | 108.8 | 107.8 | 106.4 | 106.6 |
| C1-N-C2 | 113.5 | 110.9 | 108.6 | 108.6 | 109.7 | 109.2 |
| N-C2-C2’ | 105.9 | 106.8 | 106.9 | 107.5 | 107.1 | 107.5 |
| C1-N-$C^{Ar}$ | 124.1 | 126.4 | 125.2 | 125.2 | 128.1 | 129.4 |

**REFERENCES**


i F. L. Hirshfeld, *Acta Crystallogr., Sect. A: Found. Crystallogr*., 1976, **A32**, 239.

ii D. Pham, J. C. Bertran, M. M. Olmstead, M. Mascal and A. L. Balch, *Org. Lett.,* 2005, **7**, 2805.

iii C. F. Macrae, I. J. Bruno, J. A. Chisholm, P. R. Edgington, P. McCabe, E. Pidcock, L. Rodriguez-Monge, R. Taylor, J. van de Streek, P. and A. Wood, *J. Appl. Cryst.,* 2008, **41**, 466.

iv V. Schomaker and K. N. Trueblood, *Acta Crystallogr., Sect. B: Struct. Sci.,* 1998, **B54**, 507.

v (a) A. Gavezzotti, *Acc. Chem. Res.* 1994, **27**, 309; (b) A. Gavezzotti, G. *J.* Filippini, *Phys. Chem*., 1994, **98**, 4831.

vi E. Maverick, K. Mirsky, C. B. Knobler, K. N. Trueblood and L. R. C. Barclay, *Acta Crystallogr., Sect. B: Struct. Sci.*, 1991, **B47**, 272.

vii WinGX: L. J. Farrugia, *J. Appl. Cryst*., 2012, **45**, 849.

viii E. Maverick and J. D. Dunitz, *Mol. Phys.,* 1987, **62**, 451.

ix J. D. Dunitz, E. F. Maverick and K. N. Trueblood, *Angew. Chem., Int. Ed.*, 1988, **27**, 880.

x H.-B. Bürgi, E. Blanc, D. Schwarzenbach, S. Liu, Y.-j. Lu, M. M. Kappes and J. A. Ibers, *Angew. Chem., Int. Ed.*, 1992, **31**, 640.

xi M. J. S. Dewar, E. G. Zoebisch, E. F. Healy and J. J. P. Stewart *J. Am. Chem. Soc.*, 1985, **107**, 3902.

xii J. J. P. Stewart, *J. Comput. Chem*., 1989, **10**, 209.

xiii J. J. P. Stewart, *J. Mol. Model*., 2007, **13**, 1173.

xiv K. Kim and K. D. Jordan, *J. Phys. Chem*., 1994, **98**, 10089.

xv S. *J.* Grimme, *Comput. Chem*., 1994, **27**, 1787.

xvi Y. Zhao and D. G. Truhlar, *Theor. Chem. Acc.*, 2008, **120**, 215.

xvii Gaussian 09, Revision **A.1**, M. J. Frisch, G. W. Trucks, H. B. Schlegel, G. E. Scuseria, M. A. Robb, J. R. Cheeseman, G. Scalmani, V. Barone, B. Mennucci, G. A. Petersson, H. Nakatsuji, M. Caricato, X. Li, H. P. Hratchian, A. F. Izmaylov, J. Bloino, G. Zheng, J. L. Sonnenberg, M. Hada, M. Ehara, K. Toyota, R. Fukuda, J. Hasegawa, M. Ishida, T. Nakajima, Y. Honda, O. Kitao, H. Nakai, T. Vreven, J. A. Montgomery, Jr., J. E. Peralta, F. Ogliaro, M. Bearpark, J. J. Heyd, E. Brothers, K. N. Kudin, V. N. Staroverov, R. Kobayashi, J. Normand, K. Raghavachari, A. Rendell, J. C. Burant, S. S. Iyengar, J. Tomasi, M. Cossi, N. Rega, J. M. Millam, M. Klene, J. E. Knox, J. B. Cross, V. Bakken, C. Adamo, J. Jaramillo, R. Gomperts, R. E. Stratmann, O. Yazyev, A. J. Austin, R. Cammi, C. Pomelli, J. W. Ochterski, R. L. Martin, K. Morokuma, V. G. Zakrzewski, G. A. Voth, P. Salvador, J. J. Dannenberg, S. Dapprich, A. D. Daniels, Ö. Farkas, J. B. Foresman, J. V. Ortiz, J. Cioslowski and D. J. Fox, Gaussian, Inc., Wallingford CT, 2009.